Low voltage electron beam lithography in PMMA

Mehdi Bolorizadeh[a], David C. Joy[a, b]

[a]EM Facility, University of Tennessee, Knoxville, TN 37996
[b]Oak Ridge National Laboratory, Oak Ridge, TN 37831

ABSTRACT

To examine the practical limits and problems of low voltage operation, we have studied electron beam lithography (EBL) in the low (few keV) to ultra-low (E < 100eV) energy range, employing commonly used resists such as PMMA and compared the results to those from conventional high voltage processing. The direct writing was performed at low energies by our homemade scan generator and a Schottky field emission gun scanning electron microscope (SEM), used in cathode-lens mode for ultra-low voltage operation. The exposure characteristics and sensitivity of the system at these energies have been investigated using an advanced Monte Carlo simulation method. Our modeling of the lithographic process showed a significant increase in resolution and process latitude for thinner resists.

***Keywords*:** lithography, fast secondary electrons, elastic and inelastic collisions, Monte Carlo simulation

I. INTRODUCTION

Microelectronic devices are now being developed for operation at the 45 nm technology node[1]. Conventional optical lithography (photolithography) is not expected to achieve such resolution, although new techniques such as immersion photolithography may achieve the desired performance[2]. Therefore, several alternative next generation lithography schemes that can offer the desired resolution are being considered. An obvious candidate for this task is electron beam lithography.

The resolution of features written by electron beam lithography depends on many factors, most especially (1) the energy of the incident beam, and (2) the composition and geometry of the resist and substrate materials. The trend in electron beam lithography has been to increase the electron accelerating voltage to the highest possible value. In this condition, the point spread function (PSF) describing the energy deposition of the beam consists of an intense but spatially restricted core surrounded by an extended but low intensity skirt. By an appropriate adjustment of the incident dose, the resist solubility limit can be arranged to be only exceeded in the small central region, and resolutions of 20-30 nm at energies of 50-100 keV can now be achieved in optimized conditions. However, as first shown by Broers[3] (1981), even in an arbitrarily thin resist the minimum line width is ultimately determined by lateral energy deposition from fast secondary electron (FSE) generation in the resist. Because the range of FSE is a strong function of the energy of the incident electrons, in order to fabricate structures at the nanometer scale it is necessary to look at the alternative of operating at low energies, where FSE contributions should be more confined.

Operating at beam energies below 5 keV offers both advantages and disadvantages. At such energies, chromatic aberration and diffraction effects become significantly limiting so that the electron focused beam size is increased even while the interaction volume is falling. In addition, because the source brightness falls linearly with landing energy, beam currents are decreased at low voltages. However, the electron stopping power, which measures the transfer of energy from the electron to the resist, rises at about $1/E$, enhancing the efficiency of energy deposition at low voltages and more than offsetting the decreased intensity. Finally, the electron penetration depth is decreased so that thin (~≤ 50 nm) resist layers must be employed for patterning.

In this paper we report the results of experiments and Monte Carlo simulations designed to explore the issues associated with e-beam lithography at low energies (< 5keV) and ultra-low (~ 500eV) energies. Factors to be studied include (1) the magnitude of the contributions of fast secondary electrons to the energy deposition profile and the effect on the exposure dose required, and (2) the spatial extent of the composite energy deposition profile and its effect on spatial resolution and proximity effects. In Sec. III, the simulation will be explained in more detail.

The simulations are highly developed at this time; the laboratory work is in process. Additional data would be presented at the conference.

II. EXPERIMENT

For the purposes of this analysis, PMMA has been chosen as the resist. Although more advanced materials are certainly available, PMMA is a convenient generic system whose properties are well characterized and whose performance is generally compatible with that of any proprietary resist. Layers of PMMA from below 40 nm up to about 90 nm thick were spun onto Si substrates and hard baked at 180°C for 90 sec. Their thickness was determined by a Filmetrics F20 reflectometer[4] and by step height measurements using an MFP-3DTM atomic force microscope[5] (AFM). The exposure tool was a Hitachi S-

4300 SE/N, a Schottky emitter scanning electron microscope (SEM) that can be operated from 100 eV (in cathode-lens mode) to 30 keV and in which the spot size of the electron beam can be less than 4 nm at 1 kV, and less than 2 nm at 30 kV[6]. The incident current was measured with a Faraday cup mounted on a sample stage so that the beam dose could be precisely controlled. Patterning was controlled by an external homemade pattern generator. External electron-magnetic interference with the beam was minimized by using a short working distance (~ 4 mm).

To make writing the patterning and finding the pattern easier, a gold frame was made (7 mm × 7mm) and the patterns were written inside the frame. All the beam electron-optical alignment was made on a high atomic number (Z) material like gold that was electron-beam evaporated on Si with the same thickness of the resist. Having a high Z material for height reference made the beam alignment at low and ultra low energies possible. The electron beam spot size was measured by taking an image of the height reference material and then analyzing the image using the SMART[7] macro in conjunction with SCION[8] image or NIH[9] image software.

After exposure the resist was developed in a 1:3 solution of methyl-iso-butyl-ketone: isopropyl alcohol (MIBK:IPA) for 1 min. Then 10 nm of Cr was evaporated on to the wafer using an electron-beam evaporation system (base pressure ~ high 10^{-7} Torr), and finally lifted off in acetone under ultrasonic agitation. Using such an evaporation system instead of a thermal evaporation system allows us to achieve finer metal structures.

1. Critical dose and resolution test

We looked at 10 nm Cr after liftoff. An array of dots with a constant pitch was patterned on a 45 nm and an 85 nm thick layer of PMMA, with beam energies ranging from 1 keV to 25 keV. The development process was kept fixed and the dose for each voltage was adjusted to minimize the dot size. The SEM images of a few patterns are shown in Fig. 1. The resolution increases with increasing voltage. For the 85 nm PMMA thickness at 1 keV the metal did not lift off, and we have continuous films instead of separate dots. This decrease in resolution is due to increased scattering and decreased penetration depth of low voltage electrons in the resist. Monte Carlo simulations show that 1 keV electrons are scattered laterally up to 25 nm, much more than the higher energy electrons. In addition, the electron range is only about 55 nm at 1 keV, so the resist did not develop completely. The penetration depth at 2 keV is increased to 120 nm, thus clearing the resist. This test shows that it is possible to achieve sub-200 nm resolution for 2 kV in 85 nm of PMMA, but thinner resists are needed for higher resolution or lower voltage.

2. Charging Effects

Charging is expected to be more severe at low voltages due to more efficient electron stopping in the resist. Nevertheless, we did not observe any obvious charging effects, which would show up in bending of the single pass lines near a square—a large charged area. We believe that the increased sensitivity to charging is offset by reduced resist thickness, which does not support a large surface voltage. Electron diffusion in thin films should further eliminate charging[10].

3. Resist Thickness Effects

An array of dots was patterned on 85 and 45 nm thicknesses of PMMA with 1 keV, 2 keV and 25 keV electrons. The same dose was used for each voltage. There is almost no difference among the patterns at high voltage (Fig. 1). This is not surprising, since the 25 keV electron penetration depth is several microns, and 45 nm and 85 nm resist exposures should look essentially the same. For 2 keV, however, there is some difference as the pattern was not well developed for the 85 nm but was for the 45 nm thick resist. This is consistent with the electron penetration depths discussed in Sec. II subsection 1. This test shows that the resist thickness is critical at low voltages, and that thinner resist should be used for reliable patterning.

III. MONTE CARLO SIMULATION

For optimal high resolution lithography, the beam must just only penetrate the resist in order to minimize the effect of backscattering and the consequent broadening arising from interactions within the substrate. The key factor in determining penetration is the stopping power, that is the rate (eV/A°) at which the electron deposits its energy into the medium through which it is passing. Because there is no measured stopping power data for PMMA[11], values were estimated using the Joy and Luo[12] low energy modification of the Bethe formalism[13]. Finally, it is assumed that the resist will be chemically processed in the standard way to develop the latent image for subsequent patterning of the substrate. In this case the data of Adesida et al.[14] shows that the lower limit of energy deposition in PMMA is required to produce solubility is 10^{22} eV/cm^3. For any region lying above this dose, the profile of the developed resist can then be derived from the string theory of Greeneich and van Duzer[15].

Under these assumptions, the required resist thicknesses were found to be 11nm at 1keV, 4nm at 500 eV, and about 1.5 nm at 100 eV. Note, however, that the estimated range at 100 eV maybe pessimistic because the fast secondary and backscattered electrons generated within the resist will have a longer range than the incident electrons. It is impracticable to deposit such a thin layer over large areas, and as we decrease the resist thickness, the number of defects increases.

1. Modeling The Electron-Solid Interaction

The spatial distribution of energy deposition in the resist was computed using a Monte Carlo simulation. Conventional Monte Carlo models of electron-solid interactions assume that the spatial distribution of the electrons is determined solely by elastic scattering, and that the energy deposition is determined from the continuous slowing down approximation (i.e. the Bethe stopping power equation[13]). If this model were totally correct, then for the simplest case of an unsupported thin film of resist a feature of arbitrarily small dimension could be fabricated. The lateral scattering of the beam falls to zero as the thickness of the resist decreases. In fact, as first demonstrated by Broers[3], the thickness of a line dose not fall steadily but instead reaches a limiting lower value as the resist thickness is decreased. This is because of the production of fast secondary electrons in the resist. Their initial trajectories lie almost normal to the direction of the incident electron, and as a result it is these electrons that are responsible for most of the energy deposition in the near entry surface region of the resist.

For the purposes of this study a Monte Carlo model incorporating FSE production was employed (Murata et al.[16], Joy[17]). The program uses a parametrically modified Rutherford scattering cross-section to describe elastic interactions at low beam energies, and the Evans cross-section for FSE production. The Joy and Luo[12] modification of the Bethe[13] stopping power equation was used to determine the instantaneous energy deposition. The program operates as a double Monte Carlo. The incident electron is tracked in the usual way as it travels through the resist, but at each interaction a random number is used to determine whether the interaction is elastic or inelastic (i.e. producing a FSE). If the interaction is inelastic, then the energy of the FSE generated is determined, and this electron is then tracked until it either comes to rest or leaves the specimen. Tracking the incident electron is then resumed after accounting for the energy transferred in the inelastic collision.

In order to achieve statistically valid results, between 30,000 and 100,000 trajectories were modeled for each set of conditions. Fig. (2) shows a trajectory plot from this program for the case of a 5 keV beam entering a PMMA layer 45 nm in thickness. As a result of the elastic scattering that they suffer, the incident electron trajectories (shown in blue) can be seen to fan out as the beam penetrates into the resist. The FSE trajectories shown in red typically leave the incident trajectory at an angle close to 90 degrees, thus traveling approximately parallel to the sample surface. Because these electrons are of lower energy than the incident electrons, they have a higher stopping power. Consequently, energy deposition around the beam impact point and close to the surface is dominated by the FSE contribution.

2. Results For A Point Source

Fig. 3(a) shows the radial distribution of the deposited energy within a resist layer 100 nm thick from a 5 keV point source beam. Note that the length scales in the horizontal and vertical directions are different. The plot has been color coded to produce counters of equal deposition. The scale shown above the figures is calibrated in units representing the relevant percentage of the pick energy deposition. It can be seen that under these conditions the energy profile fans out as the beam broadens during its passage through the resist. The first contour (corresponding to 30% of the pick energy deposited in any voxel) occupies a cylindrical region about 10 nm wide about the beam axis and delineates the area where the effect of the energy deposited by the FSE is the dominant term. Outside of this there is a second contour (at 10% of pick dose) that is conical in shape and broadens from 10 nm at the beam entrance surface out to about 50 nm at the exit surface. This is the region where the energy comes mostly from the scattered incident electrons. Each subsequent counter, representing a further half decay (3×'s) reduction in energy deposition, has a similar conical form leading to a further, but modest, increase in the maximum lateral wide of the profile which ultimately extends for a total wide of 250 nm.

Fig. 3(b) shows the corresponding plot for 10 nm of PMMA exposed at 1 keV. The beam is now only just penetrating the resist and consequently the energy profile is significantly different to that shown in the first example. Note that the appearance of these energy deposition profiles varies from that displayed by a more familiar presentations. This is because it is conventional to present such data by projecting the three dimensional distribution onto the plane that includes the incident beam axis, a procedure that masks the true form and symmetry of the profile. The counter representing the 30% level (red) has now shrunk to an approximately spherical region only 10 nm or so in diameter and positioned 10 nm below the entry surface. The counter for the 10% of the peak level (blue) has an open umbrella shape that can be seen to extend about 3 nm to 5nm out from the beam axis and to penetrate though about one third to one half of the thickness of the resist layer. This shape arises because the electrons have, on average, been sufficiently scattered by this depth to be diverging from the axis. The 3% and subsequent lower level counters have the more familiar apple-shape as the electron distribution continues to diffuse away from the axis.

Fig. 3(c) shows the corresponding situation for a 500 eV point source incident on a 4 nm resist layer. The shape of the energy deposition profile is very similar to that for the 1 keV case because the angular scattering of the electrons is not strongly sensitive to the actual incident energy. Consequently, under the condition in which the resist thickness is chosen so as to be equal to the beam range, then the form of the energy deposition profile can be assumed to remain constant. However the total width will vary as about $E^{1.66}$.

Fig. 4 plots the peak energy deposited in the PMMA as a function of the incident beam energy. As the energy is reduced from 3 keV to below 500 eV, the deposited energy density rises by five orders of magnitude from 10^{17} eV/cm^3/el., and the dose required to expose the resist therefore falls very rapidly as the energy is reduced, thus permitting a speeding up of the lithography. For a given electron emitter, however, the maximum current available at the focused probe falls approximately linearly with the beam energy, thus overall, lowering the incident beam energy from a few keV to a few hundred eV can be expected to improve writing speed by a factor of about 10,000×'s.

3. Feature Profiles And Exposure Sensitivity For A Point Source

Using the data of the type shown in Fig. 3 and Fig. 4, and the string model, the cross section profile of the feature that will be produced in the resist when the latent image is developed can be predicted together with the dose required to achieve it. The dose required to ensure solubility of the exposed PMMA during development is 10^{22} eV/cm^3/el. Any region dosed above this value will be assumed to be untouched by the developer. The predicted cross-sectional shape and size for 10 nm of PMMA exposed by a 1 keV beam of infinitely small size (i.e. the point source situation illustrated in Fig. 3(b)) after exposure and development an incident dose of 600 electrons would result in a hole with a U-shaped cross-section about 10 nm in diameter at the surface extending down to about 6 nm in depth, while increasing the dose to 20000 electrons would give a hole about 20 nm in total width and extending through the whole depth of the resist.

While this is an unrealistic situation, it does provide basic information on the exposure behavior of the system. For example, in Fig. 5 one can see that as the exposure dose is increased, the feature width initially increases very quickly; then it rises at a reduced rate and eventually reaches a saturation condition where the width remains constant, independent of any further increase in exposure. This would be the correct condition to target for routine exposure because it ensures the critical dimensions will not be affected by any random changes in beam intensity.

For a beam impacting 4 nm layer of PMMA at 500 eV (the situation shown in Fig. 3(c)), the behavior of the system is similar, but as shown in Fig. 5 the saturation dose required has fallen by almost a factor of ten times while the maximum feature width has fallen by only a factor of three times. Thus while writing a pattern would be much faster at 500 eV, even allowing for the decrease in current available from the source at a lower energy, the gain in resolution would be less dramatic. The lateral scattering of the FSE and the consequent energy deposition from the FSE set a lower limit to the size of the exposed region, and this varies only slowly with the incident beam energy.

References

[1] The International Technology Roadmap for Semiconductors
[2] T. Itani, W. Wakamiya, J. Cashmore, and M. Gower, Microelectron. Eng. 67-68, 39 (2003)
[3] A. N. Broers, J. Electrochem. Soc., 128, 166 (1981)
[4] http://www.filmetrics.com
[5] http://www.asylumresearch.com/Products/Mfp3D/Mfp3D.shtml
[6] http://www.hitachi.com
[7] D. C. Joy, J. of Microscopy 208, 24 (2002)
[8] http://www.scioncorp.com/
[9] http://rsb.info.nih.gov/nih-image/Default.html
[10] M. A. McCord and T.H. Newman, J. Vac. Sci. Technol. B 10, 3083 (1992)
[11] A tabulated database of measured stopping powers can be found at http://pciserver.bio.utk.edu. For a discussion of this data see D. C. Joy, S. Luo, R. Gauvin, P. Hovington, and N. Evans, Scanning Microscopy 10, 653 (1996)
[12] D.C. Joy and S. Luo, Scanning 11, 176 (1989)
[13] H. Bethe, Ann. Phys. 5, 325 (1930)
[14] I. Adesia, T. E. Everhart, and R. Shimizu, J. Vac. Sci. Technol. 16, 1743 (1979)
[15] J. S. Greeneich, and T. van Duzer, IEEE Trans. Elec. Devices 21, 286 (1974)
[16] K. Murata, D. F. Kyser, and C. H. Ting, J. App. Phys. 52, 4396 (1981)
[17] D. C. Joy, Microelectron. Engineering 1, 103 (1983)

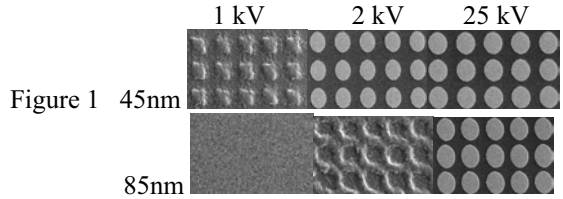

Figure 1

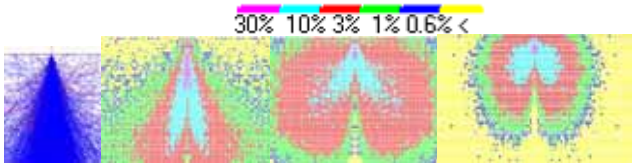

Figure 2 Figure 3(a) Figure 3(b) Figure 3(c)

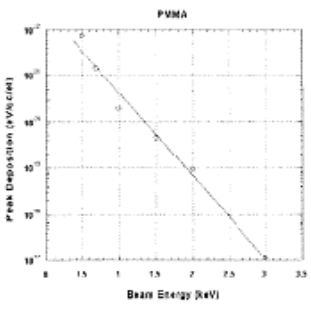

Figure 4

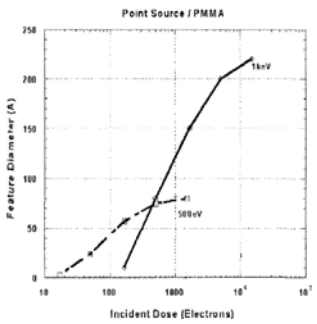

Figure 5